Hairpin Folding of Subunit *c* of F_1F_o ATP Synthase: ^1H Distance Measurements to Nitroxide-Derivatized Aspartyl-61†

Mark E. Girvin and Robert H. Fillingame*

Department of Biomolecular Chemistry, University of Wisconsin, Madison, Wisconsin 53706

Received October 7, 1993; Revised Manuscript Received November 4, 1993®

ABSTRACT: Subunit *c* from the F_1F_o ATP synthase of *Escherichia coli* folds in a hairpinlike structure of two α-helices in a solution of chloroform–methanol–H_2O, and thus resembles the structure predicted for the folded protein in the membrane. The relevance of the structure in solution to the native structure was demonstrated. Asp61 in the second helical arm was shown to retain its unique reactivity with dicyclohexylcarbodiimide (DCCD) in chloroform–methanol–H_2O solution. Further, the protein purified from the Ile28→Thr DCCD-resistant mutant proved to be less reactive with DCCD in solution. This suggested that the protein folded with Ile28 of the first helical arm close to Asp61 in the second helical arm. Subunit *c* in wild-type *E. coli* membranes was specifically labeled with a nitroxide analog of DCCD (NCCD), and the derivative protein was purified. DQF COSY spectra were recorded, and the distances between the paramagnetic nitroxide and resolved protons in the spectra were calculated based upon paramagnetic broadening of the ^1H resonances. The paramagnetic contribution to T_2 relaxation in the NCCD-labeled sample was calculated by an iterative computer-fitting method, where a control spectrum of a phenylhydrazine-reduced sample was broadened until the line shape of one-dimensional slices through each COSY cross-peak maximally mimicked the line shape of the paramagnetic sample. The distances calculated from paramagnetic broadening indicate that Ala24 and Ala25 in helix-1 lie close (ca. 12 Å) to the derivatized Asp61 in helix-2. A model for the interaction of helices in the NCCD-modified protein was generated by restrained molecular mechanics and molecular dynamics using 25 distances of <10–20 Å derived from paramagnetic broadening in combination with 15 long-range nuclear Overhauser enhancement (NOE) restraints (2–5 Å) for distances between helices and the 89 intrahelical NOEs that defined helical structure in the DCCD-modified protein.

The F_1F_o ATP synthase couples H^+ translocation through the F_o moiety in the membrane to ATP synthesis or hydrolysis at an active site in F_1 that may lie greater than 50 Å from the surface of the membrane (Senior, 1988; Fillingame, 1990). A large body of genetic and chemical evidence suggests that the smallest subunit of F_o (subunit *c* in *Escherichia coli*) is involved in both the translocation of protons and the coupling of proton translocation to ATP synthesis via conformational changes (Fillingame, 1990; Fillingame et al., 1992). Subunit *c* is thought to fold in the membrane as a hairpin of two hydrophobic α-helices connected by a more polar loop. Conserved residues in the polar loop have been shown to be necessary for conformational coupling to F_1 (Mosher et al., 1985; Fraga & Fillingame, 1989; Miller et al., 1989). A conserved carboxyl group in the middle of the C-terminal helix (Asp61 in *E. coli*) is absolutely required for H^+ translocation and is thought to protonate and deprotonate as H^+ is transported. Mutation of Asp61 to Asn or Gly results in complete loss of H^+ translocation activity (Hoppe & Sebald, 1984). These Asp61 mutations also indirectly affect the coupling of F_o with F_1 (Fillingame et al., 1984). In addition, *N*,*N*′-dicyclohexylcarbodiimide (DCCD)[1] modification of Asp61 alters substrate binding in catalytic sites and blocks conformational changes in F_1 resulting from substrate binding (Penefsky, 1985; Matsuno-Yagi et al., 1985). These effects must all be mediated by conformational changes that are transmitted from F_o to F_1. Information on the structure of the Asp61 region of subunit *c*, and the effects of Asp61 modification on the structure of the polar loop, will be of obvious mechanistic interest.

We have previously presented an initial analysis of the secondary structure and hairpinlike folding of purified subunit *c*, based on ^1H NMR data (Girvin & Fillingame, 1993). Here, we show that the purified protein retains key biochemical features observed for the protein in the native F_o complex. The unique reactivity of Asp61 with DCCD is preserved, and the rate of this reaction is reduced by the I28T substitution, a substitution causing DCCD-resistance *in vivo*. In addition, we have analyzed the structure of the protein specifically modified at Asp61 with a nitroxy analog of DCCD (NCCD). The paramagnetic nitroxy group broadened assigned ^1H resonances in both transmembrane helix-1 and transmembrane helix-2, providing further proof for hairpinlike folding. Distance ranges or limits from the nitroxide group were calculated for 54 assigned ^1H resonances, based upon increases in ^1H relaxation rates due to the paramagnetic center. A molecular model for the interaction of the two helices was constructed using these results.

† This study was supported by U.S. Public Health Service Grant GM-23105 from the National Institutes of Health. The National Magnetic Resonance Facility at Madison, supported by NIH Grant RR02301, was used in these studies. Equipment in the facility was purchased with funds from the University of Wisconsin, the NSF Biological Instrumentation Program (Grant DMB-8415048), the NIH Biomedical Research Technology Program (Grant RR02301), the NIH Shared Instrumentation Program (Grant RR02781), and the U.S. Department of Agriculture.

® Abstract published in *Advance ACS Abstracts*, January 1, 1994.

[1] Abbreviations: 1D, one dimensional; 2D, two dimensional; $\Delta\nu_{1/2}$, resonance line width at half-height; COSY, 2D correlated spectroscopy; DCCD, *N*,*N*′-dicyclohexylcarbodiimide; DQF, double quantum filtered; *J*, coupling constant; NCCD, *N*-(2,2,6,6-tetramethylpiperidine-1-oxy)-*N*′-cyclohexylcarbodiimide; NOE, nuclear Overhauser effect; NOESY, 2D NOE spectroscopy; T_2, spin–spin relaxation time; τ_c, correlation time.

0006-2960/94/0433-665$04.50/0

EXPERIMENTAL PROCEDURES

NCCD Synthesis. NCCD was synthesized essentially as described by Azzi et al. (1973). 4-Amino-2,2,6,6-tetramethylpiperidine-1-oxyl (Molecular Probes, Eugene, OR) was dissolved at 0.5 g in 2 mL of diethyl ether, and was added by drops to a solution of 1.5 mL of cyclohexyl isothiocyanate in 6.5 mL of diethyl ether and mixed gently. The reaction was allowed to proceed overnight without stirring at 20 °C. The reddish-yellow crystals were removed and washed with petroleum ether, with a yield of 93% (0.85 g) of the *N*-(2,2,6,6-tetramethylpiperidine-1-oxyl)-*N'*-(cyclohexyl)thiourea intermediate. The carbodiimide was prepared by dissolving 0.3 g of the thiourea intermediate in 30 mL of dried 2:1 benzene–pyridine and refluxing for 90 min with 1.5 g of mercuric oxide. After filtration, the benzene–pyridine was removed by evaporation, and NCCD was extracted from the residue with petroleum ether. NCCD was crystallized by evaporation of most of the petroleum ether. The yield of the carbodiimide from the thiourea was 0.265 g (98%).

Isolation of Subunit c. Wild-type subunit *c* and the subunit *c* mutants A24S and I28T were purified from *E. coli* strains LW99, RF7, and DC25, as described previously (Girvin & Fillingame, 1993). The D61G mutant was prepared from strain MM457 (Fillingame et al., 1984).

Subunit *c* was modified with NCCD as described for DCCD (Girvin & Fillingame, 1993), except that dithiothreitol was excluded from all solutions, and 2 mM potassium ferricyanide was included to prevent reduction of the nitroxide. Membranes from LW99 cells were suspended at 10 mg/mL, and treated with 0.5 μmol/mL NCCD for 45 min at 30 °C, and then with an additional 0.5 μmol/mL NCCD for 60 min. Subunit *c* was extracted with 6 volumes of 1:1 chloroform–methanol per milliliter of membranes with stirring for 2 h at 4 °C. The solvent ratio was then adjusted to 8:4:3 chloroform–methanol–water to initiate a separation of aqueous and organic phases. The lower organic phase was concentrated, and subunit *c* was purified as described previously (Girvin & Fillingame, 1993). The NCCD treatment resulted in 95% inhibition of membrane ATPase activity, and 60% modification of subunit *c*. ATPase activity was measured as described by Hermolin and Fillingame (1989).

DCCD Modification of Purified Subunit c in Solution. Dicyclohexyl[^{14}C]carbodiimide stock solution was prepared by evaporating the toluene from the [^{14}C]DCCD as it came from the manufacturer (57 mCi/mmol; Amersham Corp., Chicago, IL), and redissolving it along with nonradioactive DCCD to a final concentration of 10 mM, 1.67 mCi/mmol, in methanol. Purified subunit *c* was diluted to 0.1 mM (i.e., 0.4 mg/mL by Lowry assay using bovine serum albumin as the standard) in chloroform–methanol–water (4:4:1). [^{14}C]-DCCD was added and allowed to react for 2 h at 30 °C with continuous mixing. The reaction was stopped by cooling the samples to –20 °C, and the samples were then analyzed by HPLC within 2 h. The DCCD-modified and unmodified forms of subunit *c* were separated on an AX300 anion-exchange HPLC column (Synchropak, Linden, IN) using an ammonium acetate gradient in chloroform–methanol–water (4:4:1) as described by Hermolin and Fillingame (1989). Protein elution was monitored at 280 nm. The relative modification by DCCD was determined either by measuring the areas of the modified and unmodified peaks from the strip chart recordings or by scintillation counting of fractions from the gradient. The radioactivity in the modified peak was normalized to the total amount of protein eluted, as determined from the sum of all protein peak areas. In order to hydrolyze esters formed between carboxyl groups and solvent methanol, some samples were made 0.15 N in NaOH (by addition of 4 N NaOH in methanol–water, 1:1) and stirred for 1 h at 25 °C before analysis by HPLC.

NMR Spectroscopy. The NMR samples consisted of 2 mM NCCD-modified subunit *c* dissolved in 4:4:1 C^2HCl_3–$C^2H_3O^2H$–^2H_2O, made 50 mM in NaCl, at an uncorrected pD of 6.8, prepared as described (Girvin & Fillingame, 1993). In control spectra, the nitroxide was reduced by addition of 3 mM phenylhydrazine. Phase-sensitive DQF COSY spectra were acquired at 27 °C on a Bruker AM-500 spectrometer using the pulse sequence of Rance et al. (1983). Phase-sensitive NOESY data were acquired as described by Kumar et al. (1980) and Bodenhausen et al. (1984) with a mixing time of 150 ms varied randomly by ±15 ms to reduce scalar coupling effects (Macura et al., 1982). The data were collected on an Aspect 3000 computer as 512 blocks of 64 (NOESY) or 128 (COSY) transients, each with 4096 time domain points, and processed on a Silicon Graphics (Mountain View, CA) Personal IRIS using Felix 2.0 software (Hare Research, Bothell, WA). The data sets were zero-filled to 4096 by 4096 data points before Fourier transformation. No resolution-enhancing window functions were used for the COSY spectra. A shifted sine bell was applied to both the t_1 and t_2 dimensions of the NOESY spectrum.

Measurement of T_{2P}. The paramagnetic contribution to T_2 relaxation in NCCD-labeled subunit *c* was determined by an iterative fitting procedure adapted from a suggestion of Kosen (1989). In the suggested procedure, a narrower control spectrum is broadened until the difference between it and the broader sample spectrum is zero. This method is not directly applicable to 2D spectra in general, and phase-sensitive COSY spectra in particular, because the amplitude of a cross-peak does not depend on a single T_2 parameter. Hence, the procedure was modified by scaling the broadened control spectrum to have the same maximal amplitude as the paramagnetic sample spectrum, so that only the line shapes, and not maximal intensities, would be used in determining T_{2P}.

Corresponding 1D slices through all assigned cross-peaks were extracted from COSY spectra of the control (NCCD nitroxide reduced by phenylhydrazine) and paramagnetic sample (oxidized) NCCD-labeled subunit *c*. The range of data points unique to the cross-peak of interest was determined manually. A program was written to determine the best fit for the increase in line width.[2] The cross-peak being fit was extracted from both 1D slices using a trapezoidal window to eliminate contributions from neighboring resonances. Both slices were zero-filled to 8192 data points, and the sample spectrum was shifted by 1 or 2 points, as required, to align it properly with the control spectrum. The control spectrum was inverse Fourier transformed, multiplied with an exponential decay with a varying time constant (T_{2P}), Fourier transformed, scaled to the same maximal intensity as the sample spectrum, and subtracted from the control, and the difference between the two was squared and summed. The value of T_{2P} was decreased in large steps until the control was broader than the sample. The value for T_{2P} giving the best fit was determined by essentially a binary search on T_{2P}, minimizing on the sum of squares of the differences between sample and control spectra until the change in $\Delta\nu_{1/2P}$ ($=1/\pi T_{2P}$) was less than 0.05 Hz.

Molecular Modeling. The transmembrane portion of NCCD-modified subunit *c* was modeled using the programs

[2] The software described runs under MS-DOS, and is available upon request from the authors.

Insight and Discover (Biosym Technologies, San Diego, CA) on a Personal IRIS. The two transmembrane segments (Asp7–Leu36 and Arg50–Ala79) were initially constructed as α-helices based on the NOE data from a previous study (Girvin & Fillingame, 1993). Restrained molecular mechanics simulations (Mackay et al., 1989) were first performed on both helices individually, using the CVFF molecular force field and a dielectric constant of 10. The intrahelical NOEs were used as the restraints, with a distance range of 2.0–5.0 Å, force constants of 50 kcal/Å, and a maximum limit of 100 kcal. The NCCD was built and attached to Asp61. Both possible attachment sites (N and N′) and several starting NCCD orientations were examined. Distances from the nitroxide to protons in helix-2 were used as restraints during the simulations of NCCD-modified helix-2, and the lowest energy (also the least distorted) conformation was selected.

The 2 helices of the protein were brought together by restrained molecular mechanics and dynamics simulations from 10 different starting antiparallel alignments of the helices. In these starting structures, the centers of the two helices were separated by at least 50 Å, resulting in minimal distances between side chains in the two helices of 40 Å. In the initial starting structure, Asp61 was facing toward Ala24 and Ile28, and positioned at the same height along the helix axis, as suggested by genetic experiments (Hoppe et al., 1980b; Miller et al., 1990; Fillingame et al., 1991). Additional starting alignments were generated by tilting helix-2 by ±30° with respect to helix-1, as well as by translating the tilted helix-2's up and down 25 Å along the direction of the helical axis of helix-1. Helix-2 was also rotated about its axis by ±90° in the starting antiparallel alignment. The distance restraints included the following: NOEs from the 2,6H of Phe35 to the H^{α} and H^{γ} of Thr51, and to the H^{β} of Phe54 observed in the DCCD-modified protein (Girvin & Fillingame, 1993); NOEs involving the 2,6H of Tyr10, Tyr73, and Phe76 observed in the NCCD-modified protein in the present work (see Table 2); distances from the nitroxide of NCCD to ^1H in helix-1 and helix-2 calculated from relaxation data (Table 1). All interhelical restraints were given initial force constants of 25 kcal/Å, and the maximum energy for each restraint was initially limited to 10 kcal to prevent excessive distortion of the molecule during the simulation. Each pair of helices was subjected to repeated iterations of 1000 cycles of mechanics (energy minimization, steepest descents algorithm) and 1000 steps of dynamics (1.0 fs each at 500 K), with the force constants on the restraints increased by 25 kcal/Å until a maximum of 250 kcal/Å was reached. A quadratic bond potential function was used, charges were ignored, and cutoff distances for all interactions were set to 150 Å. At this point, all distance restraints had been satisfied. All terms and potentials were set to their normal values, a dielectric constant of 10 was assumed, and each molecule was further minimized using conjugate gradients until the maximum derivatives were less than 0.001 kcal/(mol·Å).

RESULTS

Aspartyl-61 of Isolated Subunit c Specifically Reacts with DCCD. In the native F_o of *E. coli*, Asp61 of subunit *c* is uniquely reactive with DCCD. This reactivity is greatly diminished by mutation of residues 24 and 28 in the adjacent transmembrane helix (Hoppe et al., 1980b; Fillingame et al., 1991). We examined the reaction of DCCD with purified wild-type and mutant forms of subunit *c* to see if the conformation giving rise to these unique properties was retained in chloroform–methanol–water solvent.

Wild-type subunit *c* was treated with DCCD in chloroform–methanol–water solution, and the reaction products were separated by anion-exchange HPLC (Figure 1A). DCCD treatment of the wild-type protein gave rise to two reaction products. The second of these (product II, eluting at 17.5 min) coeluted with the radioactivity from [^{14}C]DCCD, and corresponded in elution position to the DCCD-modified form of the protein isolated from DCCD-treated membranes. We presume the first product (eluting at 16.5 min) to be a methyl ester formed between the DCCD-activated Asp61 carboxyl group and solvent methanol since product I, but not product II, was unstable to NaOH treatment. Because of the interference from the methyl ester, we quantified the DCCD modification by totaling the ^{14}C radioactivity in the product II fractions, with normalization for protein applied by dividing by the total area of all protein peaks.

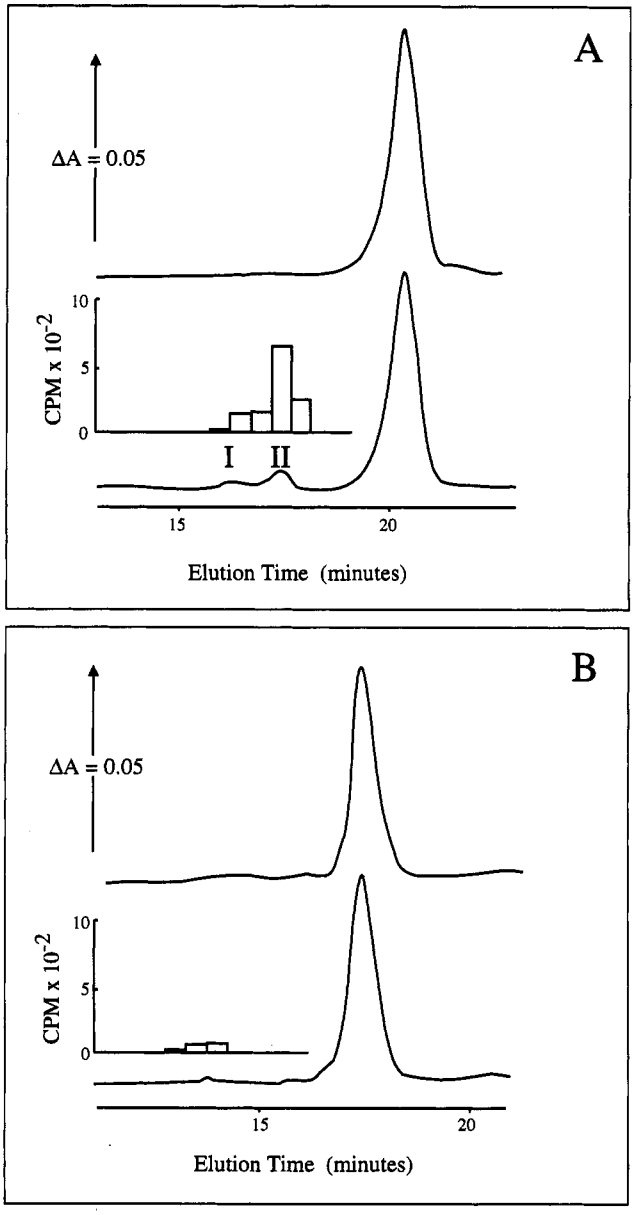

FIGURE 1: Anion-exchange HPLC of purified subunit *c* for (A) wild-type subunit *c* and (B) D61G mutant subunit *c*. Upper traces are for untreated protein, and lower traces are for protein treated with 250 μM [^{14}C]DCCD for 2 h at 30 °C in chloroform–methanol–water, 4:4:1. The inset above each lower trace shows the radioactivity determined for each 0.5-min fraction. Elution time is measured from the beginning of the gradient.

To determine whether the modification was occurring at Asp61 or one of the other five carboxyl groups of the protein, we performed the same experiment using a mutant in which Gly is substituted for Asp61 (Hoppe et al., 1980a). DCCD

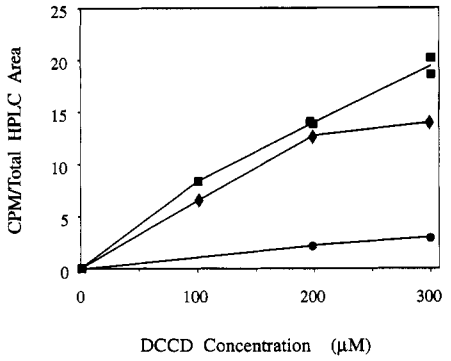

FIGURE 2: Incorporation of [^{14}C]DCCD into purified subunit *c*. Purified (■) wild-type, (●) D61G, and (♦) A24S mutant subunits *c* were modified with varying concentrations of [^{14}C]DCCD, and the modified and unmodified forms were separated as described for Figure 1. The reaction conditions were otherwise identical to those described for Figure 1. Radioactivity in the modified protein was determined by liquid scintillation counting and normalized to the total amount of subunit *c* eluted, measured as the sum of all protein peak areas. Samples with incorporation of 20 cpm/total HPLC peak area correspond to approximately 5% modification of the total subunit *c* present.

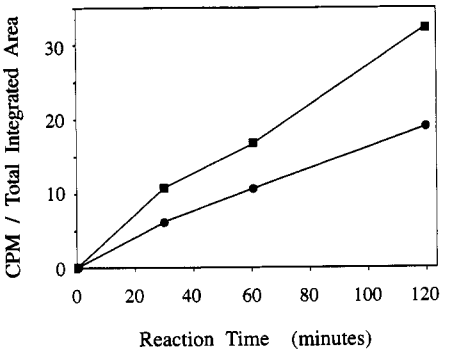

FIGURE 3: Time course of incorporation of [^{14}C]DCCD into purified subunit *c*. Purified (■) wild-type and (●) I28T mutant subunits *c* were treated with 300 μM DCCD. The reaction conditions were otherwise identical to those described for Figure 1.

modification of subunit *c* was abolished in membranes of this mutant (Altendorf & Zitzmann, 1975). As shown in Figures 1B and 2, the isolated D61G mutant protein reacts much less readily than the wild-type protein with DCCD. We presume that the basal rate of modification represents nonspecific reaction at carboxyls other than Asp61 in the protein. An NaOH-sensitive product was not observed with the D61G mutant protein, and this may indicate that product I observed with the wild-type protein was an Asp61 adduct.

The DCCD reactivities of two DCCD-resistant subunit *c* mutants were examined. The reactivity of the A24S mutant was comparable to wild type (Figure 2). Typically there was slightly less (5–15%) modification of the mutant by DCCD with respect to the wild-type protein, but the difference was not proven to be statistically significant. The I28T mutant, on the other hand, was substantially more resistant to modification by DCCD. Figure 3 shows the time course of the modification of isolated wild-type and I28T mutant subunit *c* by 300 μM DCCD. The rate of DCCD modification of the mutant is half that of wild type. Similar differences were observed when the extent of modification was measured as a function of DCCD concentration as in Figure 2 (data not shown).

Modification of Asp61 of Subunit c by NCCD. We have previously reported a 2D ^{1}H NMR analysis of isolated subunit *c* (Girvin & Fillingame, 1993). Because of the extreme resonance overlap observed for this predominantly helical protein, we were unable to make complete resonance assignments and define the structure of the protein from NOE data. An alternative approach to measuring distances in a protein by NMR is to attach a paramagnetic center at a specific location, and measure the increase in the T_2 relaxation rates ($1/T_2$) of assigned resonances due to paramagnetic relaxation (Schmidt & Kuntz, 1984). The increase in T_2 relaxation can be determined from the increase in proton resonance line widths. The paramagnetic contribution to T_2 relaxation (T_{2P}) falls off as the inverse sixth power of the distance from the paramagnetic center. In a small protein, resonances from protons within 9–10 Å of the paramagnetic group will be broadened beyond detection, while those in the range of 10–20 Å will be broadened by 0.5–20 Hz, depending on the distance from the probe.

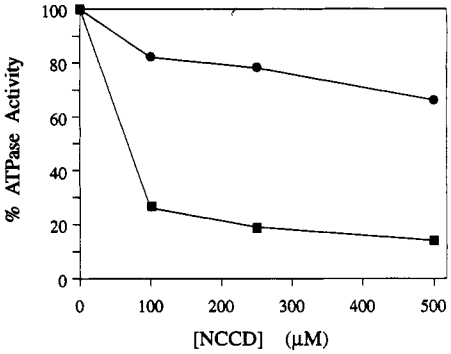

FIGURE 4: Inhibition of *E. coli* membrane ATPase by NCCD. ATPase activities of *E. coli* inner membrane vesicles of (■) wild-type and (●) A24S mutant subunits *c*. Membranes, suspended at 10 mg/mL, were treated with NCCD for 30 min at 30 °C.

Azzi et al. (1973) have synthesized a nitroxide-containing analog of DCCD (NCCD), in which 2,2,6,6-tetramethylpiperidine-1-oxyl replaces one of the cyclohexyl rings of DCCD, and used this compound to examine the mobility and exposure of the reactive carboxyl of the mitochondrial DCCD binding subunit. We initially hoped to use this compound to provide information on distances between helix-1 and helix-2 of *E. coli* subunit *c*, before we had proven the hairpin model by other NMR measurements. We first needed to verify that the NCCD probe reacted specifically with Asp61 of subunit *c*. The inhibitory effect of NCCD on the ATPase activity of *E. coli* inner membrane vesicles is shown in Figure 4. The membrane ATPase could be inhibited nearly completely by NCCD treatment. A 20-fold higher concentration of NCCD, relative to DCCD, was required to achieve equivalent inhibition. The specificity of the reaction for Asp61 of subunit *c* was indicated by the greatly reduced reactivity of NCCD with the A24S protein in membranes of a DCCD-resistant mutant (Figure 4).

For the NMR experiments, intact F_o in *E. coli* inner membranes was modified with NCCD under essentially the same conditions used in Figure 4. Subunit *c* was then purified, and the modified and unmodified forms were separated by anion-exchange chromatography. The modified form of the protein was transferred to deuterated solvent for NMR spectroscopy. Several differences between NCCD-labeled and unlabeled subunit *c* were evident even in 1D spectra. The ε-methyl resonances of two Met residues (presumably Met57 and Met65 which flank Asp61) and the aromatic proton resonances of Phe53 and Phe54 were absent from the spectrum of the labeled protein (Figure 5A). Other resolved resonances, such as the aromatic protons of Tyr10 and Tyr73, were unaffected by the nitroxide. Reduction of the nitroxide with phenylhydrazine restored the Met and Phe resonances (Figure 5B).

Distances of Assigned Protons from the Nitroxide of NCCD. The resolution of a 2D experiment was required to

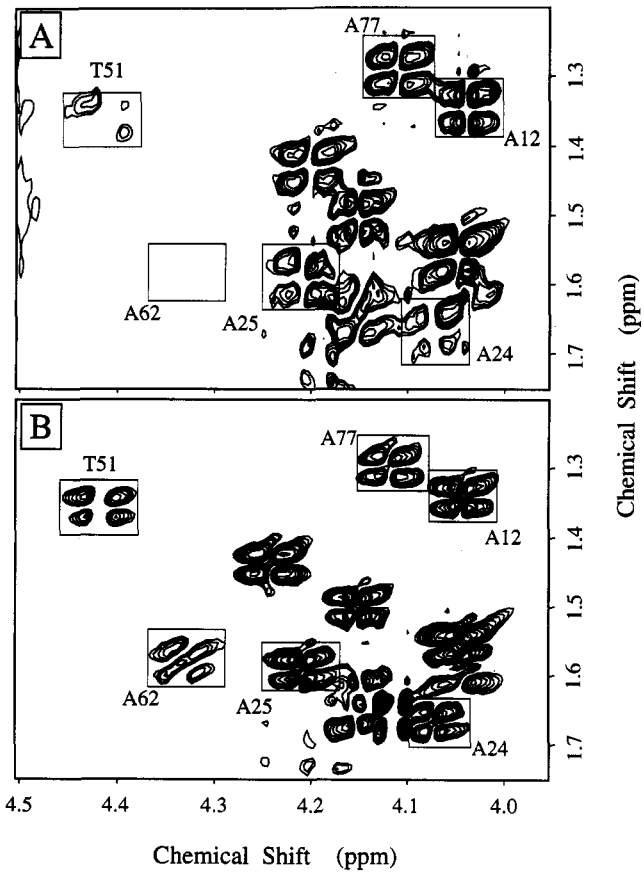

FIGURE 7: Expansion of the Ala $\alpha\beta$ region of the DQF COSY spectra of oxidized (A) and reduced (B) NCCD-modified subunit *c*. Note in particular the reduction in intensity of the Ala24 and Ala25 (first helix residues) cross-peaks in the oxidized sample (A) relative to the reduced control (B).

downfield (in t_1) cross sections were fit, and each was fit using three separate window widths. All calculated broadenings agreed to within 10%. In addition, the calculated best fits for several resonances were varied by ±5, 15, 25, and 33%, and these generated line shapes were compared with the calculated fits and the sample spectra. Figure 9 shows the sample Thr51 H^{γ} resonance along with the control resonance broadened by the calculated best fit (9.8 Hz), and by the best fit ±33% (13.1 and 6.6 Hz). Although the fitting process appeared to be accurate to within 10–15%, a more generous error limit range of ±33% was used for the calculation of distance ranges.

Distances from the unpaired electron of the nitroxide to each of the measured proton resonances were calculated from the equation for paramagnetic relaxation:

$$\Delta\nu_{1/2P} = \frac{1}{\pi T_{2P}} = \frac{S(S+1)\gamma_I^2 g^2 \beta^2}{15r^6}\left(4\tau_c + \frac{3\tau_c}{1+\omega_I^2\tau_c^2}\right)$$

(Solomon, 1955; Bloembergen, 1957), where S, γ_I, g, and β are physical constants for the proton and electron, ω_I is the frequency of the proton resonance, τ_c is the correlation time for the molecule, and r is the distance between the proton and the unpaired electron. Using the 1.9-ns value for τ_c determined by Montecucco and Azzi (1975) for the isolated NCCD-modified subunit of mitochondria in chloroform–methanol, and substituting in the other parameters, the equation reduces to

$$r\ (\text{Å}) = \sqrt[6]{4.31 \times 10^7/\Delta\nu_{1/2P}}$$

The values of r calculated from this equation for each of the fitted resonances are shown in Table 1.[3] Line-width increases

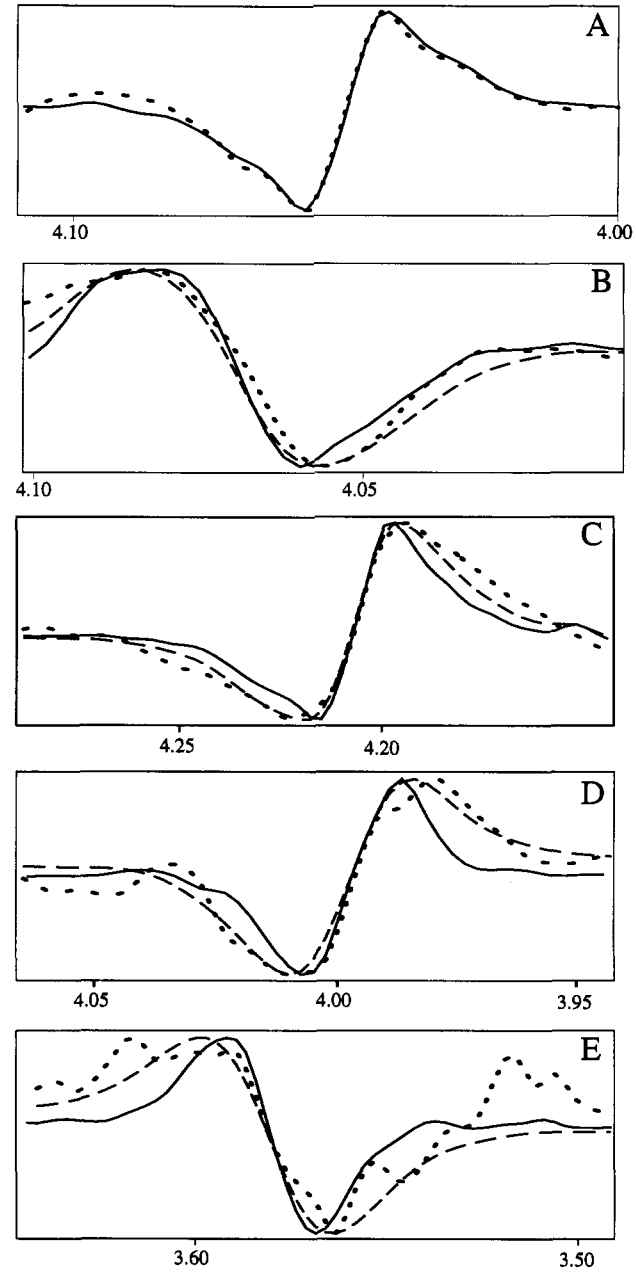

FIGURE 8: Fits of the increase in line width due to paramagnetic relaxation for several H^{α} resonances from both helices. One-dimensional (t_2) slices through the H^{α} dimension of the $H^{\alpha\beta}$ cross-peaks of Ala12 (A), Ala24 (B), Ala25 (C), Thr51 (D), and Val56 (E). Shown for each are cross sections of the control (phenylhydrazine reduced) sample (—), the paramagnetic sample (···), and the best computer fit of a broadened control t_2 slice to the sample t_2 slice (- - -).

of less than 1.0 Hz were not used for distance calculations. Also shown in Table 1 are the upper and lower distance limits used for molecular modeling. For protons exhibiting measurable paramagnetic relaxation, these were calculated from the above equation after adding and subtracting 33% to the experimentally determined $\Delta\nu_{1/2}$ values. Because of the inverse sixth root dependence of the calculated distance on $\Delta\nu_{1/2}$, even the large error limits used resulted in a range of distance uncertainties of only 1.2–2.2 Å. Protons which were broadened beyond detection were assumed to be within a range of 2–12

[3] The value of r is relatively insensitive to changes in τ_c. For example, a 2-fold error in τ_c would result in an 8.5% error in r.

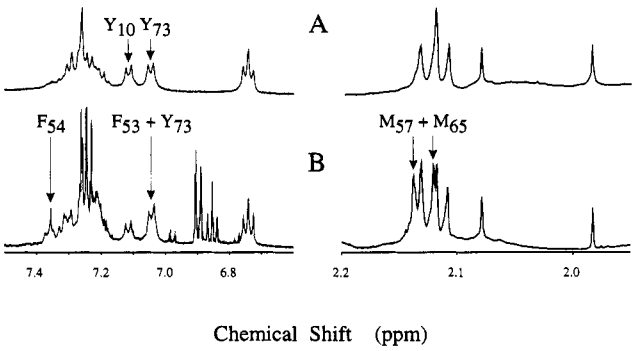

FIGURE 5: Expansions of one-dimensional 500-MHz ^{1}H NMR spectra of oxidized and reduced NCCD-modified subunit *c*. The aromatic side-chain and methionine ϵ-methyl resonances are shown before (A) and after (B) addition of 3 mM phenylhydrazine to reduce the paramagnetic nitroxide. The additional unlabeled resonances in the aromatic region of (B) were from the added phenylhydrazine.

analyze the effects of the paramagnetic probe in any detail. The changes in line shapes could have been determined from almost any 2D NMR experiment. We chose to analyze DQF COSY spectra because the antiphase multiplet cross-peaks provided the best resolution of partially overlapped resonances. In the DQF COSY spectra, at least one or two components of the multiplets of neighboring cross-peaks could be resolved and fitted for most assigned resonances of subunit *c* (e.g., see Tyr10 and Phe53 in Figure 6B). For control spectra, the nitroxide was reduced to the hydroxylamine by a 1.5 molar excess of phenylhydrazine (Lee & Keanna, 1975). Neither ascorbic acid nor dithionite was effective in reducing the nitroxide, presumably because of their low solubility in organic solvent.

The effect of the nitroxide on the $\alpha\beta$-proton cross-peaks of the Asp, Asn, Phe, and Tyr residues can be seen in Figure 6A,B. The Asp61 resonances visible in the reduced control (6B) were broadened beyond detection by the nitroxide (6A) while the other Asp and Asn resonances were not broadened. Two residues near Asp61 were also strongly affected: the Phe54 resonances were dramatically reduced in intensity, and those from Phe53 were not detectable. Residues near the N- and C-termini (Tyr10, Tyr73, and Phe76) were unaffected by the nitroxide.

The Ala $\alpha\beta$- and Thr $\beta\gamma$-proton cross-peaks are shown in Figure 7A,B. Again, residues near in sequence to Asp61 were obviously affected by the nitroxide (e.g., Thr51 and Ala62) while those near the N- and C-termini were not (e.g., Ala12 and Ala77). The resonances from Ala24 and Ala25 in the middle of the first transmembrane helix were slightly altered by the nitroxide. Both cross-peaks were somewhat broader (documented below), with lower intensities than in the control spectrum.

The paramagnetic contribution to T_2 relaxation was measured from 1D slices through each of the assigned resonances in the DQF COSY spectra, comparing the oxidized to the reduced sample. Choosing the method by which to measure T_{2P} was difficult. The increase in line width at half-height ($\Delta\nu_{1/2P} = 1/\pi T_{2P}$) could not be measured directly from the COSY spectra because of distortion of the line shapes due to cancellation from the antiphase multiplets. Neither could the decrease in maximal cross-peak intensity be used because of complications arising from its dependence on both $\sin(\pi J t_1)e^{-t_1/T_{2Pa}}$ in the t_1 dimension and $e^{-t_2/T_{2Pb}}$ in the t_2 dimension, as well as cancellation from the antiphase multiplets. An iterative fitting procedure was used instead, where we determined the increase in line width required to make the line shape of the control spectrum identical to the line shape of the paramagnetically broadened oxidized spectrum.

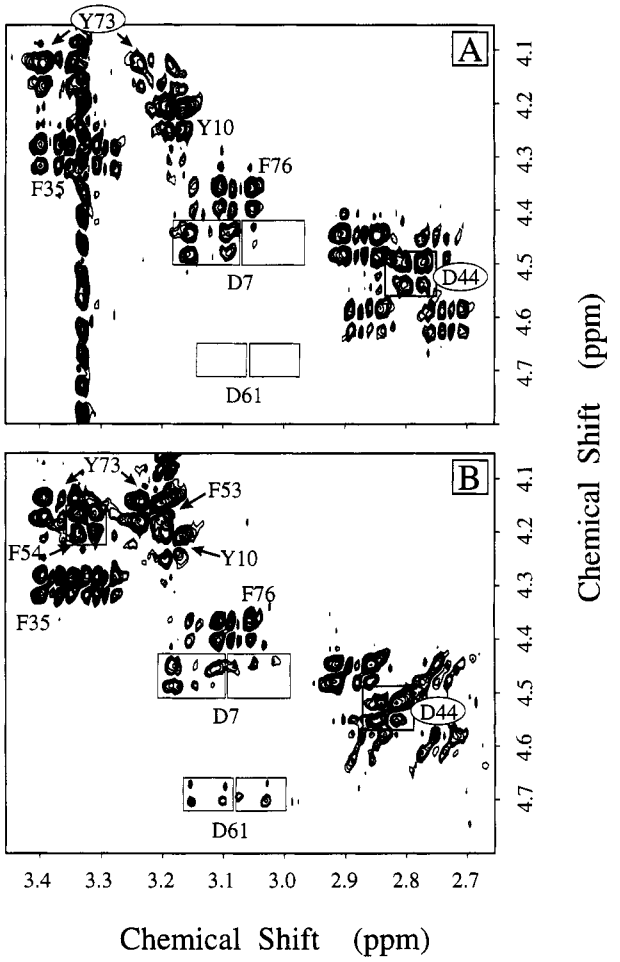

FIGURE 6: Expansion of the aromatic and Asx $\alpha\beta$ region of the 500-MHz ^{1}H DQF COSY spectra of oxidized and reduced NCCD-modified subunit *c*. Assigned resonances are labeled. Note the absence of the Phe53, Phe54, and Asp61 cross-peaks (second helix residues) in the oxidized sample (A), and their reappearance in the reduced control (B).

All proton resonances which had been resolved and assigned were fit. Examples of the fitting for several H^α are shown in Figure 8, and for the H^γ of Thr51 in Figure 9. In Figure 8, the spectra of the paramagnetically broadened sample, the reduced control, and the best fit of the artificially broadened control to the sample are all superimposed. The range of paramagnetic broadening shown is from 0 Hz for Ala12 (Figure 8A), through 9.6 and 5.4 Hz for Ala24 and Ala25 (Figure 8B,C), to 19.5 and 28.7 Hz for Thr51 and Val56 (Figure 8D,E). The range of line width increases which could be fitted with reasonable accuracy was from about 1 Hz (not shown) to 30 Hz (e.g., Figure 8E for Val56 where the signal intensity is reduced almost to that of the noise). The results from fitting all assigned resonances which could be resolved are shown in Table 1. Paramagnetic broadening was observed for the residues in the second helix flanking Asp61 (Arg50 through Pro64), and in the first helix in residues proposed to be opposite Asp61 (Met16 through Phe35). The only anomaly noted was for the Val68 H^α and H^β resonances, which showed no measurable increase in line width even though the resonance intensities were reduced by about 40% in the paramagnetic sample. No paramagnetic broadening was detected for residues in the N- and C-termini (Asn3 through Ala12 and Leu70 through Val78) or in the polar loop (Arg41 through Asp44), although the end of the Arg41 side chain may be within the detectable relaxation range of the nitroxide. The quality of the fits was evaluated in two ways. First, for all cross-peaks except Arg50 and Met16, both the upfield and

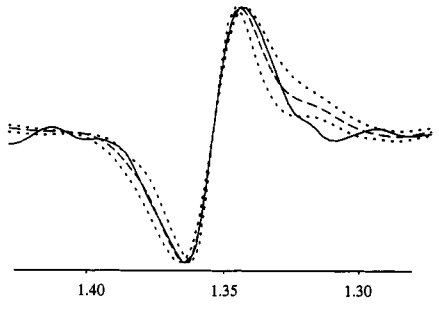

FIGURE 9: Effect of varying the calculated broadening of the control t_2 slice to fit the paramagnetic sample t_2 slice for the Thr51 H^{γ} resonance. Shown are the one-dimensional (t_2) slice through the Thr51 $H^{\beta\gamma}$ cross-peak of the paramagnetic sample spectrum (—), the control spectrum broadened by the calculated best-fit line-width increase of 9.8 Hz (- - -), and control spectra broadened by the calculated best-fitting line-width increase ±33%, i.e., 6.6 and 13.1 Hz (···).

Å of the probe, while protons with resonances showing no effect were assumed to be greater than 20 Å distant from the probe. The only exception was for Val68. Although the Val68 H^{α} and H^{β} did not appear to be broadened by oxidized NCCD, the unexplained reduction in intensity of their cross-peak suggested lowering the minimum distance used to 16 Å.

Interhelical NOE Cross-Peaks in NCCD-Modified Subunit c. A NOESY spectrum of NCCD-modified subunit *c* was examined to ensure that the protein was folded, as well as to obtain as many additional restraints as possible for molecular modeling. As with the unmodified protein, the only resolvable, unambiguous interhelical NOE cross-peaks involved the aromatic side chains. The general pattern of interhelical NOE connectivities between the C- and N-termini of the protein was similar to that of the unmodified protein (Table 2), indicating that the modified protein also folds as two antiparallel helices. The set of protons giving rise to the NOEs did differ slightly from that of the unmodified protein (e.g., cross-peaks between Tyr73 2,6H and Met16 H^{β} in the unmodified protein, but between Tyr73 2,6H and Met17 H^{β} and H^{γ} in the NCCD-modified protein). Thus, minor differences in structure of the NCCD-modified and unmodified protein should be expected when the final structures are solved. As expected, no cross-peaks were observed involving Phe35, Phe53, or Phe54 because of relaxation from the nitroxide.

Modeling the Transmembrane Region of Subunit c. A model of the membrane-embedded region of NCCD-modified subunit *c* was generated by a combination of restrained molecular mechanics and dynamics using the distances obtained from NOE measurements and nitroxide broadening as the restraints. The distance restraint ranges used were 2–5 Å for NOEs, and the minimum and maximum distances listed in Table 1 for paramagnetic relaxation derived distances. Both membrane-spanning segments were initially built as α-helices, based on previous NOE results for Asp7 through Ile26 and Arg50 through Ile55, and Ala67 through Ala77 (Grivin & Fillingame, 1993). The NCCD group was constructed and attached to Asp61 via either N or N′, in several starting geometries. Restrained molecular mechanics simulations were then performed on the NCCD-labeled C-terminal helix using both the intrahelical NOE distances and paramagnetic relaxation derived distance ranges as restraints. The lowest energy model, which was also the least distorted structure, was one in which the *N*-acylurea of NCCD was formed by attachment of the N adjacent to the piperidyl ring rather than the N′ adjacent to the cyclohexyl ring. The nitroxide-bearing piperidyl ring was located adjacent to Met57 and Gly58. All distance restraints were satisfied by this conformation. The N-terminal helix was also simulated using intrahelical NOEs as restraints. Starting structures were then generated by positioning the 2 helices 50 Å apart in 10 different antiparallel arrangements. Totals of 15 interhelical and 89 intrahelical NOEs, 13 interhelical and 12 intrahelical paramagnetic relaxation distance ranges, and 29 distance limits (greater than 20 Å) were used in the molecular simulations (Figure 10).

Table 1: ^1H Line-Width Increases, Calculated Distance Restraints from NCCD, and Distances in Molecular Model of NCCD-Modified Subunit *c*

resonance	fitted line-width increase (Hz)	calcd distance from NCCD (Å)	modeling restraint (Å)		distance from NCCD in model (Å)
			min distance	max distance	
D7 H^{α}	0.0	>20.0	20.0	50.0	30.1
D7 H^{β}	0.0	>20.0	20.0	50.0	28.7
Y10 H^{α}	0.0	>20.0	20.0	50.0	24.1
Y10 H^{β}	0.0	>20.0	20.0	50.0	26.1
M11 H^{α}	0.0	>20.0	20.0	50.0	25.5
A12 H^{α}	0.0	>20.0	20.0	50.0	21.7
A12 H^{β}	0.0	>20.0	20.0	50.0	23.3
V15 H^{α}	0.2	24.1	20.0	50.0	20.9
V15 H^{β}	1.0	18.8	17.9	20.1	20.1
V15 H^{γ}	0.2	24.1	20.0	50.0	23.1
M16 H^{α}	1.7	17.2	16.4	18.4	16.4
M16 H^{β}	1.0	18.7	17.8	20.0	17.8
A24 H^{α}	9.6	12.8	12.2	13.7	12.5
A24 H^{β}	7.3	13.4	12.8	14.4	12.8
A25 H^{α}	5.4	14.1	13.5	15.1	14.5
A25 H^{β}	3.8	15.0	14.3	16.0	16.0
K34 H^{α}	10.3	12.7	12.1	13.6	13.6
K34 H^{β}	8.3	13.2	12.5	14.1	13.5
K34 H^{δ}	3.6	15.1	14.4	16.2	14.5
K34 H^{ϵ}	3.7	15.1	14.4	16.1	15.7
F35 H^{α}	2.7	15.9	15.1	17.0	15.9
F35 H^{β}	2.6	15.9	15.2	17.0	15.8
R41 H^{α}	0.4	21.5	20.0	50.0	nm[a]
R41 H^{β}	0.0	>20.0	20.0	50.0	nm
R41 H^{γ}	0.1	27.5	20.0	50.0	nm
R41 H^{δ}	3.7	15.0	14.3	16.1	nm
D44 H^{α}	0.3	23.6	20.0	50.0	nm
D44 H^{β}	0.0	>20.0	20.0	50.0	nm
R50 H^{α}	33.2	10.4	10.0	11.2	10.0
T51 H^{α}	19.5	11.4	10.9	12.2	11.0
T51 H^{β}	10.9	12.6	12.0	13.4	13.4
T51 H^{γ}	9.8	12.8	12.2	13.7	12.8
F53 $H^{\alpha,\beta}$	nd[b]	<12.0	>2.0	<12.0	5.2
F54 $H^{\alpha,\beta}$	nd	<12.0	>2.0	<12.0	6.2
V56 H^{α}	28.7	10.7	>2.0	<12.0	5.4
G58 $H^{\alpha,\alpha'}$	nd	<12.0	>2.0	<12.0	9.0
V60 H^{α}	73.2	9.2	>2.0	<12.0	5.8
D61 $H^{\alpha,\beta}$	nd	<12.0	>2.0	<12.0	7.9
A62 $H^{\alpha,\beta}$	nd	<12.0	>2.0	<12.0	10.7
P64 $H^{\alpha,\beta}$	nd	<12.0	>2.0	<12.0	10.4
V68 H^{α}	0.0	>20.0	16.0	50.0	17.2
V68 H^{β}	0.0	>20.0	16.0	50.0	15.2
L70 H^{α}	0.0	>20.0	20.0	50.0	20.0
Y73 H^{α}	0.0	>20.0	20.0	50.0	23.7
V73 H^{β}	0.0	>20.0	20.0	50.0	21.6
V74 H^{α}	0.0	>20.0	20.0	50.0	25.9
V74 H^{β}	0.1	24.1	20.0	50.0	26.2
V74 H^{γ}	0.0	>20.0	20.0	50.0	25.0
M75 H^{α}	0.0	>20.0	20.0	50.0	27.3
F76 H^{α}	0.0	>20.0	20.0	50.0	28.2
F76 H^{β}	0.1	29.9	20.0	50.0	26.0
A77 H^{α}	0.7	19.8	20.0	50.0	29.9
A77 H^{β}	0.0	>20.0	20.0	50.0	27.4
V78 H^{α}	0.0	>20.0	20.0	50.0	31.5
V78 H^{β}	0.0	>20.0	20.0	50.0	32.0

[a] Not modeled. Because of a lack of assignments and distance restraints, the polar loop region was not modeled. [b] Not detected. These broadened cross-peaks were too weak to pick out of the noise.

Table 2: Interhelical NOE Cross-Peaks in Unmodified versus NCCD-Modified Subunit *c*

from resonance	to resonance	
	unmodified subunit *c*	NCCD-modified subunit *c*
Tyr10 2,6H	Tyr73 $H^{\beta'}$	Tyr73 H^{β}
Tyr10 2,6H	Met75 H^{α}	
Tyr10 2,6H	Met75 H^{γ}	
Tyr10 2,6H	Met75 H^{γ}	Met75 H^{γ}
Tyr10 2,6H	Phe76 H^{α}	
Tyr10 3,5H		Tyr73 H^{α}
Tyr10 3,5H		Tyr73 H^{β}
Tyr73 2,6H	Tyr10 H^{β}	
Tyr73 2,6H	Met16 $H^{\beta'}$	
Tyr73 2,6H		Tyr10 H^{α}
Tyr73 2,6H		Met17 H^{β}
Tyr73 2,6H		Met17 H^{γ}
Tyr73, 2,6H		Met17 H^{γ}
Phe76 2,6H	Met17 $H^{\beta'}$	
Phe76 3,4,5H		Tyr10 H^{β}

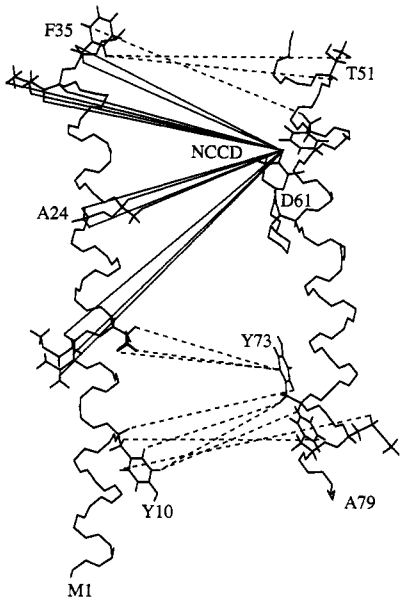

FIGURE 10: Interhelical restraints used in modeling the transmembrane region of NCCD-modified subunit *c*. The transmembrane region is shown from Met1 through Phe35 in the N-terminal helix and from Arg50 through Ala79 in the C-terminal helix. Side chains are only shown for residues involved in interhelical restraints. Dashed lines indicate NOE restraints, and solid lines indicate restraints derived from paramagnetic relaxation.

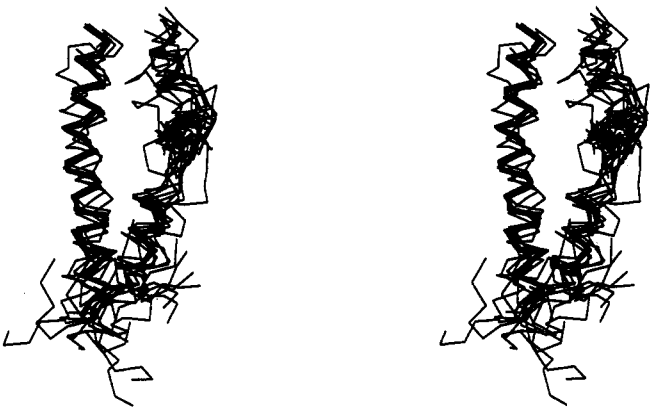

FIGURE 11: Stereo C^{α} trace of the final backbone conformations resulting from combined restrained molecular mechanics and dynamics simulations of 10 starting alignments of NCCD-modified subunit *c*. The transmembrane region is shown for each conformation from Met1 through Phe35 in the N-terminal helix and from Arg50 through Ala79 in the C-terminal helix. The piperidyl ring of NCCD is also shown for each model. The two α-carbon traces deviating significantly from the helix-2 bundle are the two highest energy models in Table 3.

Table 3: Calculated Energies and Backbone Heavy-Atom Deviations in Subunit *c* Models Resulting from Combined Restrained Molecular Mechanics and Dynamics Simulations

	model				
no.	skew angle (deg)[a]	translation (Å)[b]	rotation (deg)[c]	energy (kcal/mol)[d]	RMSD (Å)[e]
1	0	0	−90	0.8	0.98
2	0	0	90	156.6	1.09
3	−10	0	0	135.9	0.84
4	−30	0	0	112.2	0.86
5	−30	25	0	65.2	0.88
6	−30	−25	0	443.2	1.66
7	10	0	0	51.0	0.92
8	30	0	0	62.1	0.81[f]
9	30	25	0	0.0	0.90
10	30	−25	0	99.9	1.05

[a] Angle of helix-2 relative to helix-1. [b] Translation of helix-2 along helical axis of helix-1, with zero meaning Asp61 and Ala24 aligned at the same height. [c] Rotation of helix-2 about its helical axis, with zero meaning Asp61 facing directly toward Ala24. [d] Calculated energy relative to the lowest energy model (number 9). [e] Root mean squared deviations for all backbone heavy atoms in the range of residues from Tyr10–Phe35 and Arg50–Phe76 for a given model to all other models. [f] Model shown in Figure 12.

The combined restrained molecular mechanics and molecular dynamics simulations of NCCD-labeled subunit *c* resulted in a reproducible alignment of helices that was relatively unaffected by choice of starting structure (Figure 11 and Table 3). Each of the models shown satisfied all of the distance restraints. Most of the models were quite similar to each other, with the root mean squared deviations between backbone atoms in all but one of the models being less than 1 Å. Most of the variation between models occurred at the very ends of the helices, and in the region around Asp61, where no secondary structural restraints have been obtained. The model with the smallest deviations from the ensemble of models is shown in Figure 12 (the unrestrained, and hence disordered, regions from Met1–Leu9 and Ala77–Ala79 are not displayed). The distances between the nitroxide and assigned protons are compared with the ranges predicted from the NMR experiment (Table 1). The Tyr and Phe residues at the N- and C-termini of the protein appear to form an aromatic cluster, as hinted at by the observed NOE cross-peaks. The Phe residues near the polar loop, though near one another, appear less clustered. Except for a slight bulge from Ala20 through Ile22, the N-terminal transmembrane segment is helical throughout its length. Both ends of the C-terminal segment are helical, with considerable unraveling occurring between Phe54 and Pro64.

The nitroxide-bearing ring of NCCD appears fixed in a depression in the second α-helix at about the level of Gly58, surrounded in the N-terminal direction by Phe53, Phe54, and Met57 (Figure 12). This restricted mobility is suggested by the nitroxide's effect extending further in the N-terminal direction from Asp61 than in the C-terminal direction. The data fit satisfactorily with the presented model assuming that the nitroxide remains close to this position with little rotation around the intervening bonds to Asp61. A maximum occurrence of the alternate orientation of NCCD (with the positions of the rings interchanged) was estimated to be less than 20% based on the calculated effect such an orientation would have had on the resonances of Leu70 through Val74. Due to the four extra methyl groups, the ring containing the nitroxide is bulkier than the cyclohexyl ring, which may explain its preferential occupancy of this site. The depression itself

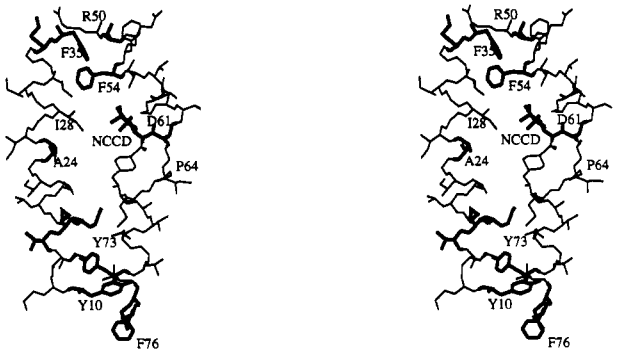

FIGURE 12: Stereo model of the transmembrane region of NCCD-modified subunit *c* derived from combined restrained molecular mechanics and dynamics. The model shown (number 8 in Table 3) had the lowest rms deviation from the ensemble of helices shown in Figure 11. The backbone is shown without oxygens, and the side chains are shown without hydrogens for clarity. The residues shown in boldface are those for which an interhelical distance restraint has been assigned. The conformation shown for other residues is that predicted by energy minimization and molecular dynamics after satisfaction of assigned distance restraints. The transmembrane region is shown from Tyr10 through Phe35 in the N-terminal helix and from Arg50 through Phe76 in the C-terminal helix.

arises from the folding of the backbone and the absence of a side chain at position 58.

DISCUSSION

The NMR experiments reported here and in an earlier study (Girvin & Fillingame, 1993) show that purified subunit *c* folds in a hairpinlike structure in chloroform–methanol–H_2O solvent, much like it is predicted to fold in the complete F_o complex in the membrane. In addition, we have shown that the Asp61 residue of the purified protein remains uniquely reactive with DCCD. The region of structure around Asp61 must therefore retain properties like that in native F_o. The reaction of DCCD with Asp61 of subunit *c* in chloroform–methanol–H_2O solvent was affected by one substitution giving rise to DCCD-resistance *in vivo*, but not by a second substitution. The reduced reactivity observed in the purified I28T protein clearly supports a close interaction between Asp61 on helix-2 and residue 28 on helix-1. However, the reactivity was only reduced by approximately 2-fold, whereas the reactivity in native F_o is probably reduced by a factor of 5–10-fold (Fillingame et al., 1991). The difference may indicate that the helix–helix interaction is more transient in chloroform–methanol–H_2O solvent. It is unclear why the purified A24S substitution shows different properties, giving rise to low DCCD reactivity in native F_o, but essentially wild-type DCCD reactivity in the purified state. This difference might again be accounted for by a transient association of helices in organic solvent, or it could indicate important structural differences between the purified protein and subunit *c* as it is found in native F_o. Alternatively, the A24S substitution may only slow reaction with DCCD when the subunits of F_o are associated. Conceivably, the A24S substitution of one subunit *c* could slow reaction with the neighboring subunit *c* molecule in the F_o complex. Recall that F_o has a subunit stoichiometry of approximately $a_1b_2c_{10\pm1}$ (Foster & Fillingame, 1982), and an interaction of *c* subunits within F_o would appear mandatory and of probable functional significance (Fillingame, 1990; Fillingame et al., 1992). The DCCD reactivity of the A24S protein in native F_o varies significantly with the carbon source used for cell growth (Fillingame & Wopat, 1978), and this suggests that minor changes in F_o structure can perturb the interaction of residue 24 with residue 61. It therefore may not be surprising that DCCD resistance is completely lost when the A24S protein is purified.

The modeling procedure provided a reproducible alignment of the two helices of NCCD-modified subunit *c*. One of the assumptions made with the starting structures was that both transmembrane segments were helical. This assumption seemed reasonable despite the lack of evidence for helical secondary structure in deuterated chloroform–methanol–water solvent for Ile28 through Phe35 and for Met57 through Ile66. In the final model, the calculated distances from the nitroxide to residues at both ends of both transmembrane segments agreed well with a helical secondary structure. No information was available about the conformation of the polar loop, other than the possibility that the side chain of Arg41 folds toward the C-terminal helix based upon data from the spin-label experiment. Hence, the loop was not modeled.

In the model, both helices are slightly curved, and cross each other at an angle of approximately 20°. The C-terminal helix shows the most curvature, probably because of insertion of the NCCD rings, and perhaps because of Pro64 in the middle of that helix. The model suggests an unraveling of helix-2 centered around the site of NCCD binding. It is presently unclear whether this unraveled section of helix-2 represents the true folding of the NCCD-modified protein or whether this is the result of performing molecular dynamics on a region where secondary structural restraints are lacking. It is possible that the unmodified protein is more helical in this region and that the unraveling reflects the conformational change expected to occur on DCCD modification of subunit *c* in the intact F_o (Penefsky, 1985). The general structures of the unmodified and modified proteins are likely to be very similar because most chemical shifts are unaffected by the modification (Girvin & Fillingame, 1993). However, minor differences in the pattern of interhelical NOE cross-peaks were observed on comparing the two forms of the protein (Table 2), and these differences suggest that there may be a slight realignment of helices on NCCD or DCCD modification.

The model provides several clues as to why the protein would form a stable hairpin in an organic solvent mixture rather than adopting an extended helical conformation. The clustering of the aromatic side chains at both ends of the transmembrane segments suggests itself as one possible stabilizing interaction. In a survey of 34 water-soluble proteins by Burley and Petsko (1985), most of the aromatic residues were observed to form clusters of 2 or more side chains, usually occurring between elements of secondary structure. They estimated that each aromatic pair contributed 1–2 kcal/mol to the stabilization of the folded protein. Many such clusters are also present in the structures of the bacterial photosynthetic reaction center (Deisenhofer et al., 1985) and bacteriorhodopsin (Henderson et al., 1990). Additional stabilization may result from the alternation and interdigitation of long and short side chains along the interface between helices. Looking from the N- and C-termini toward the polar loop in the modeled alignment, Leu9/Tyr10 are opposed to Ala77, followed by the pairs Ala13/Ala14 with Tyr73, Met16/Met17 with Gly69, Ala20/Ala21 with Met65/Ile66, a break at the region around Ala24/Ala25 and Asp61/Ala62, and then continuing with Ile28/Leu31 with Gly58. This type of pattern also occurs in the structures of the reaction center and bacteriorhodopsin, and presumably stabilizes folding by maximizing van der Waals interactions between adjacent helices as suggested by Cohen and Parry (1986) and Landschulz et al. (1988) for leucine zippers.

The model for the transmembrane portion of subunit *c* conforms with predictions made from previous chemical and genetic experiments performed on the intact complex. In the model, the protein folds as a hairpin of helices, with Ala24

and Ile28 positioned very near to Asp61. This proximity might have been anticipated from studies of DCCD-resistant mutants, as discussed above. The proximity of Asp61 to Ala24 is also predicted by the finding of Miller et al. (1990) that function is retained in an unusual double mutant, where the position of the Asp residue is exchanged between positions 61 and 24. What appears most important is that one of the two transmembrane helices anchors the functionally crucial carboxyl group at the proper position in the center of the membrane.

Another interesting feature of the model is the location of one of the rings of NCCD in a pocket, one helical turn away from Asp61, which is formed by the lack of a side chain on Gly58 and the large surrounding side chains of Phe53, Phe54, and Met57. A similar pattern for residues at positions 54, 57, and 58 is preserved in the sequences of subunit *c* from other species, where the residue at the position equivalent to Gly58 is either Gly or Ala, and the residues at positions equivalent to Phe54 and Met57 are Phe/Trp/Leu and Leu/Phe/Val, respectively. Since the unique reactivity of DCCD with the carboxyl group in the membrane has been observed in these homologous sequences, one is tempted to speculate that this pocket is important for stabilizing the interaction of DCCD with the protein long enough for the *O*-acylisourea intermediate in the reaction to rearrange to the stable *N*-acylurea product (Williams & Ibrahim, 1981).

The spin-label experiment allowed us to measure distances over a longer range than those detected in the NOESY experiment. The method provided useful results, even though complete assignments were not available. An additional benefit of the experimental approach is that the 2D resolving power of the COSY spectrum is used to separate the resonances and a third piece of information, the line shape, is used to provide the distance information. Previous calculations of distances from paramagnetic relaxation have been based on determining changes in amplitudes of resonances resolved in one dimension (Schmidt & Kuntz, 1984). The extension of this quantitative approach to two-dimensional spectra has not been straightforward due to the more complicated dependencies of the amplitude of a cross-peak relative to the resonance amplitude in one dimension. By collecting a control spectrum as suggested by Kosen (1989), and using a computer program to find the increase in relaxation rate giving the best match for each assigned resonance, a large number of distances could be derived relatively quickly from the two-dimensional spectrum. Given the current capacity to introduce specific modification sites, e.g., Cys, by site-directed mutagenesis, this spin-label approach could prove to be quite useful in exploring the structures of larger proteins.

ACKNOWLEDGMENT

The NMR experiments were carried out at the National Magnetic Resonance Facility at Madison. We thank Dr. Ken Satyshur and Dr. Dan Rich for their help with the initial modeling of subunit *c*. We thank Mary Gillis for her skilled general assistance and the analysis of the DCCD reactivity of the I28T subunit *c* mutant.

REFERENCES

Altendorf, K., & Zitzmann, W. (1975) *FEBS Lett. 59*, 268–272.
Azzi, A., Bragadin, M. A., Tamburro, A. M., & Santato, M. (1973) *J. Biol. Chem. 248*, 5520–5526.
Bloembergen, N. (1957) *J. Chem. Phys. 27*, 572–577.
Bodenhausen, G., Kogler, H., & Ernst, R. R. (1984) *J. Magn. Reson. 58*, 370–388.
Burley, S. K., & Petsko, G. A. (1985) *Science 229*, 23–28.
Cohen, C., & Parry, D. A. D. (1986) *Trends Biochem. Sci. 11*, 245–248.
Deisenhofer, J., Epp, O., Miki, K., Huber, R., & Michel, H. (1985) *Nature 318*, 618–624.
Fillingame, R. H. (1990) in *The Bacteria* (Krulwich, Ed.) Vol. 12, pp 345–391, Academic Press, New York.
Fillingame, R. H., & Wopat, A. E. (1978) *J. Bacteriol. 134*, 687–689.
Fillingame, R. H., Peters, L. K., White, L. K., Mosher, M. E., & Paule, C. R. (1984) *J. Bacteriol. 158*, 1078–1083.
Fillingame, R. H., Oldenburg, M., & Fraga, D. (1991) *J. Biol. Chem. 266*, 20934–20939.
Fillingame, R. H., Girvin, M. E., Fraga, D., & Zhang, Y. (1992) *Ann. N.Y. Acad. Sci. 671*, 323–334.
Foster, D. L., & Fillingame, R. H. (1982) *J. Biol. Chem. 257*, 2009–2015.
Fraga, D., & Fillingame, R. H. (1989) *J. Biol. Chem. 264*, 6797–6803.
Girvin, M. E., & Fillingame, R. H. (1993) *Biochemistry 32*, 12167–12177.
Henderson, R., Baldwin, J. M., Ceska, T. A., Zemlin, F., Beckmann, E., & Downing, K. H. (1990) *J. Mol. Biol. 213*, 899–929.
Hermolin, J. & Fillingame, R. H. (1989) *J. Biol. Chem. 264*, 3896–3903.
Hoppe, J., & Sebald, W. (1984) *Biochim. Biophys. Acta 768*, 1–27.
Hoppe, J., Schairer, H. U., & Sebald, W. (1980a) *FEBS Lett. 109*, 107–111.
Hoppe, J., Schairer, H. U., & Sebald, W. (1980b) *Eur. J. Biochem. 112*, 17–24.
Kosen, P. A. (1989) *Methods Enzymol. 177*, 86–121.
Kumar, A., Ernst, R. R., & Wüthrich, K. (1980) *Biochem. Biophys. Res. Commun. 95*, 1–6.
Landschulz, W. H., Johnson, P. F., & McKnight, S. L. (1988) *Science 240*, 1759–1764.
Lee, J. D., & Keanna, J. F. W. (1975) *J. Org. Chem. 40*, 3145–3147.
Mackay, D. H. J., Cross, A. J., & Hagler, A. T. (1989) in *Prediction of Protein Structure and the Principles of Protein Conformation* (Fasman, G. D., Ed.) pp 317–358, Plenum Press, New York.
Macura, S., Wüthrich, K., & Ernst, R. R. (1982) *J. Magn. Reson. 46*, 269–282.
Matsuno-Yagi, A., Yagi, T., & Hatefi, Y. (1985) *Proc. Natl. Acad. Sci. U.S.A. 82*, 7550–7554.
Miller, M. J., Fraga, D., Paule, C. R., & Fillingame, R. H. (1989) *J. Biol. Chem. 264*, 305–311.
Miller, M. J., Oldenburg, M., & Fillingame, R. H. (1990) *Proc. Natl. Acad. Sci. U.S.A. 87*, 4900–4904.
Montecucco, C., & Azzi, A. (1975) *J. Biol. Chem. 250*, 5020–5025.
Mosher, M. E., White, L. K., Hermolin, J., & Fillingame, R. H. (1985) *J. Biol. Chem. 260*, 4807–4814.
Penefsky, H. S. (1985) *Proc. Natl. Acad. Sci. U.S.A. 82*, 1589–1593.
Rance, M., Sørensen, O. W., Bodenhausen, G., Wagner, G., Ernst, R. R., & Wüthrich, K. (1983) *Biochem. Biophys. Res. Commun. 117*, 479–485.
Schmidt, P. G., & Kuntz, I. D. (1984) *Biochemistry 23*, 4261–4266.
Sebald, W., Machleidt, W., & Wachter, E. (1980) *Proc. Natl. Acad. Sci. U.S.A. 77*, 785–789.
Senior, A. E. (1988) *Physiol. Rev. 68*, 177–231.
Solomon, I. (1955) *Phys. Rev. 99*, 559–565.
Williams, A., & Ibrahim, I. T. (1981) *Chem. Rev. 81*, 589–636.